ELSEVIER

Neurobiology of Disease

www.elsevier.com/locate/ynbdi
Neurobiology of Disease 28 (2007) 30 – 38

Selective vulnerability of cerebral white matter in a murine model of multiple sclerosis detected using diffusion tensor imaging

Shu-Wei Sun,[a,*] Hsiao-Fang Liang,[a] Robert E. Schmidt,[b] Anne H. Cross,[c] and Sheng-Kwei Song[a]

[a] *Department of Radiology, Washington University School of Medicine, St. Louis, MO, USA*
[b] *Department of Pathology and Immunology, Washington University School of Medicine, St. Louis, MO, USA*
[c] *Department of Neurology, Washington University School of Medicine, St. Louis, MO, USA*

Received 23 December 2005; revised 5 June 2007; accepted 8 June 2007
Available online 23 June 2007

In this study, axial ($\lambda_{\parallel}$) and radial ($\lambda_{\perp}$) diffusivities derived from diffusion tensor imaging (DTI) were used to evaluate white matter injury in brains of mice affected by experimental autoimmune encephalomyelitis (EAE). Sixteen female C57BL/6 mice were immunized with amino acids 35–55 of myelin oligodendrocyte glycoprotein ($MOG_{35–55}$). Three months after immunization, optic nerve and tract were severely affected with 19% and 18% decrease in $\lambda_{\parallel}$ respectively, suggesting the presence of axonal injury. In addition, a 156% and 86% increase in $\lambda_{\perp}$ was observed in optic nerve and tract respectively, suggestive of myelin injury. After *in vivo* DTI, mice were perfusion fixed and immunohistochemistry for the identification of myelin basic protein (MBP) and phosphorylated neurofilament (pNF) was performed to verify the presence of axonal and myelin injury. The present study demonstrated that the visual pathway is selectively affected in $MOG_{35–55}$ induced murine EAE and these injuries are non-invasively detectable using $\lambda_{\parallel}$ and $\lambda_{\perp}$.

Keywords: EAE; MOG; DTI; Visual pathway; Optic nerve; Optic tract; Mouse brain; Axonal damage; Myelin damage; Directional diffusivity

Introduction

Multiple sclerosis (MS) is an inflammatory demyelinating disease of the central nervous system (CNS). It is the second leading cause of neurological disability in young adults. Although the prevailing consensus of the pathogenesis of MS is that it results from a coordinated attack of the immune system against the primary constituents of white matter (Whitney et al., 1999), increasing evidence suggests that axonal damage plays a significant role in the neurological dysfunction suffered by MS patients (Kornek and Lassmann, 2003; Kornek et al., 2000). Axonal damage occurs in areas of demyelinating lesions (Ferguson et al., 1997; Trapp et al., 1998) as well as white matter tracts distant from demyelinated plaques (Davie et al., 1997; Fu et al., 1998; Trapp et al., 1998). Identification and differentiation of myelin and axonal damage in MS is crucial to understand these pathological processes and to develop more effective therapies.

Experimental autoimmune encephalomyelitis (EAE) is a widely used animal model of human MS. The EAE model mimics many aspects of human MS (Conlon et al., 1999; Raine, 1984; Raine and Traugott, 1984). For example, EAE induced by myelin oligodendrocyte glycoprotein (MOG) reproduces the presumed pathophysiological processes of MS including both the encephalitogenic T-cell response and the demyelinating autoantibody response (Iglesias et al., 2001; Kornek et al., 2000; Linington et al., 1993; Storch et al., 1998). Similarities between MOG-EAE and MS of axonal pathologies, and phagocytosis by microglia and macrophages have also been demonstrated (Craner et al., 2005; Kornek et al., 2000).

Magnetic resonance imaging (MRI) has been used extensively as a sensitive, objective, and quantifiable measure of pathology and therapeutic responses in MS patient management. MS plaques are typically multiple, localized predominantly to CNS white matter, and bright on T_2-weighted and Fluid Attenuated Inversion Recovery (FLAIR) images. The abnormalities observed on brain MRI are pathologically nonspecific, and may result from a spectrum of potential pathology, including edema, demyelination, gliosis, and inflammation (Guttmann et al., 1995). Improved specificity has been achieved using contrast enhanced T_1-weighted imaging to identify active lesions of inflammation in EAE and MS (Morrissey et al., 1996; Rovaris and Filippi, 2000; Yousry et al., 2000). However, none of these MRI measures are capable of differentiating axonal and myelin injury (Meier et al., 2004).

Recently, the directional diffusivities of water molecules in white matter derived using MR diffusion tensor imaging (DTI)

* Corresponding author. Biomedical MR Laboratory, Campus Box 8227, Washington University School of Medicine, 660 S. Euclid Avenue, St. Louis, MO 63110, USA. Fax: +1 314 362 0526.
E-mail address: richard@bmr.wustl.edu (S.-W. Sun).
Available online on ScienceDirect (www.sciencedirect.com).

0969-9961/$ - see front matter © 2007 Elsevier Inc. All rights reserved.
doi:10.1016/j.nbd.2007.06.011

have been proposed and demonstrated that axonal injury in white matter results in reduced axial diffusivity ($\lambda_{\|}$) while myelin damage increases radial diffusivity ($\lambda_{\perp}$) without changing $\lambda_{\|}$ (Kim et al., 2006; Song et al., 2002, 2003, 2005; Sun et al., 2006a, b). In this study, directional diffusivities derived from DTI were employed to investigate the pattern of axonal and myelin injury in chronic EAE induced by $MOG_{35–55}$ peptide in mouse brain. Histology was performed afterwards to validate the *in vivo* DTI findings. Our results showed that the visual pathway is severely affected in $MOG_{35–55}$ peptide induced chronic EAE and directional diffusivities may be used to non-invasively identify and characterize these lesions.

Methods

Animal preparation

Eight-week-old female C57BL/6 mice were randomly separated into two groups: 16 in the experimental group and 16 in the control group. Mice in the experimental group were immunized with $MOG_{35–55}$ peptide (M-E-V-G-W-Y-R-S-P-F-S-R-V-V-HL-Y-R-N-G-K), synthesized by Peptide Synthesis Facility, Washington University, St. Louis, MO) (Lyons et al., 1999). Active EAE was induced by immunization of mice with 50 μg $MOG_{35–55}$ emulsified (1:1) in complete Freund's adjuvant (CFA). Pertussis toxin (300 ng; PTX, List Laboratories, Campbell, CA) was injected intravenously on the day of immunization and 3 days later. Animals were graded daily for clinical disability on a scale of 0–5 (Cross et al., 1994). At 3 months after immunization, when the mice were chronically affected, *in vivo* DTI of brains was performed on all mice of both experimental and control groups.

In vivo DTI of mouse brains

Mice were anesthetized with a mixture of oxygen and isoflurane (Baxtor Healthcare Corporation, IL, USA) using an isoflurane vaporizer (D. R. C., Inc., KY, USA). Core body temperature was maintained at 37 °C using warm water circulating in a pad. Mice were placed in a holder to immobilize the head. A 9-cm inner diameter Helmoltz coil served as the RF transmitter. A 1.5-cm outer diameter circular surface coil was employed as the RF receiver. The entire device was placed in an Oxford Instruments 200/330 magnet (4.7 T, 33-cm clear bore) equipped with a 15-cm inner diameter, actively shielded Oxford gradient coil (18 G/cm, 200-ìs rise time). The magnet, gradient coil, and Techron gradient power supply were interfaced with a Varian UNITY-INOVA console controlled by a Sun Microsystems Ultra-60 Sparc workstation. A spin-echo, diffusion-weighted imaging sequence was employed to acquire diffusion-weighted images. The acquisition parameters were repetition time (TR) 1.7 s, spin echo time (TE) 45 ms, time between application of gradient pulses (Δ) 25 ms, diffusion gradient duration (δ) 8 ms, 4 scans averaged per *k* space line (3 h total), slice thickness 0.5 mm, field of view 3.0 cm, data matrix 256×256 (zero filled to 512×512). Images were obtained with diffusion sensitizing gradients applied in six directions: [Gx, Gy,Gz]=[1,1,0], [1,0,1], [0,1,1], [−1,1,0], [0,−1,1], and [1,0,−1]. The *b* values used were 0 and 0.847 ms/μm^2. On a pixel-by-pixel basis, quantitative indices, including axial diffusivity ($\lambda_{\|}$), radial diffusivity ($\lambda_{\perp}$), relative anisotropy (RA), and trace of the diffusion tensor (Tr), were derived using software written in Matlab (MathWorks, Natick, MA, USA) defined by the following equations (Basser and Pierpaoli, 1996; Song et al., 2005; Sun et al., 2003):

$$\mathrm{Tr} = \lambda_1 + \lambda_2 + \lambda_3 \tag{1}$$

$$\lambda_{\|} = \lambda_1 \tag{2}$$

$$\lambda_{\perp} = 0.5 \times (\lambda_2 + \lambda_3) \tag{3}$$

$$\mathrm{RA} = \frac{\sqrt{(\lambda_1 - \mathrm{Tr}/3)^2 + (\lambda_2 - \mathrm{Tr}/3)^2 + (\lambda_3 - \mathrm{Tr}/3)^2}}{\sqrt{3}(\mathrm{Tr}/3)} \tag{4}$$

Regions of interest (ROI) were manually defined using the mouse brain atlas (Franklin and Paxinos, 1997) as the reference. Taking the advantage that T_2-weighted images (T_2WI, the images with no diffusion weighting) and DTI index maps were spatially co-registered with same resolution in our data acquisition, the combination of the image contrasts from T_2WI and DTI could provide informative anatomical landmarks to ensure the consistency of ROI selection between animals. Thus, T_2WI and parametric maps of the DTI indices (RA, Tr(D), $\lambda_{\|}$, and $\lambda_{\perp}$) were displayed and used to guide the selection of the ROI from each slice of the multi-slice data. Six white matter tracts were measured including anterior commissure (AC), corpus callosum (CC), cerebral peduncle (CP), external capsule (EC), optic nerve (ON), and optic tract (OT) (Fig. 1). These ROI were then combined across slices to yield a single volume-averaged value for each tract. Although DTI indices changed in optic nerve and optic tract in EAE-affected mice, these changes did not reduce the image contrast necessary to delineate ROI. For example, $\lambda_{\perp}$ provides significant contrast against the cerebrospinal fluid (CSF) surrounding the ON from both EAE and control mice (Song et al., 2003; Sun et al., 2006a). Similarly, T_2WI offers superb contrast between OT and surrounding tissues in both control and EAE mice. The strategy of ROI analysis has proven reproducible in consistently detecting neurological injury in our hands (Sun et al., 2003, 2005, 2006a). Data were presented as mean±standard deviation (N=6). A two-tailed *t*-test was performed to compare the measurements between control and experimental groups. Statistical significance was accepted at $P<0.05$.

Immunohistochemistry evaluation

Cross sectional examinations were performed to histologically validate the *in vivo* DTI findings. At the conclusion of *in vivo* DTI examinations, mice (N=7) were perfusion fixed through left cardiac ventricle with phosphate buffered saline (PBS) followed by 4% paraformaldehyde in PBS. The intact brain was excised, placed in 4% paraformaldehyde/PBS for 2 weeks and transferred to PBS for storage at 4 °C until histological analysis (*ca.* 1 week).

A 4-mm-thick coronal section (−1 to +3 mm of bregma) was obtained from each brain and embedded in paraffin. 3-μm-thick slices matching the DTI images were cut and deparaffinized in xylene for immunohistochemical examinations. Hematoxylin and eosin (H&E) staining was performed. In addition, the integrity of axons was evaluated using a primary antibody against phosphorylated neurofilament (pNF, SMI-31, 1:1000; Sternberger Monoclonals, Lutherville, Maryland) (Sun et al., 2006b) and myelin

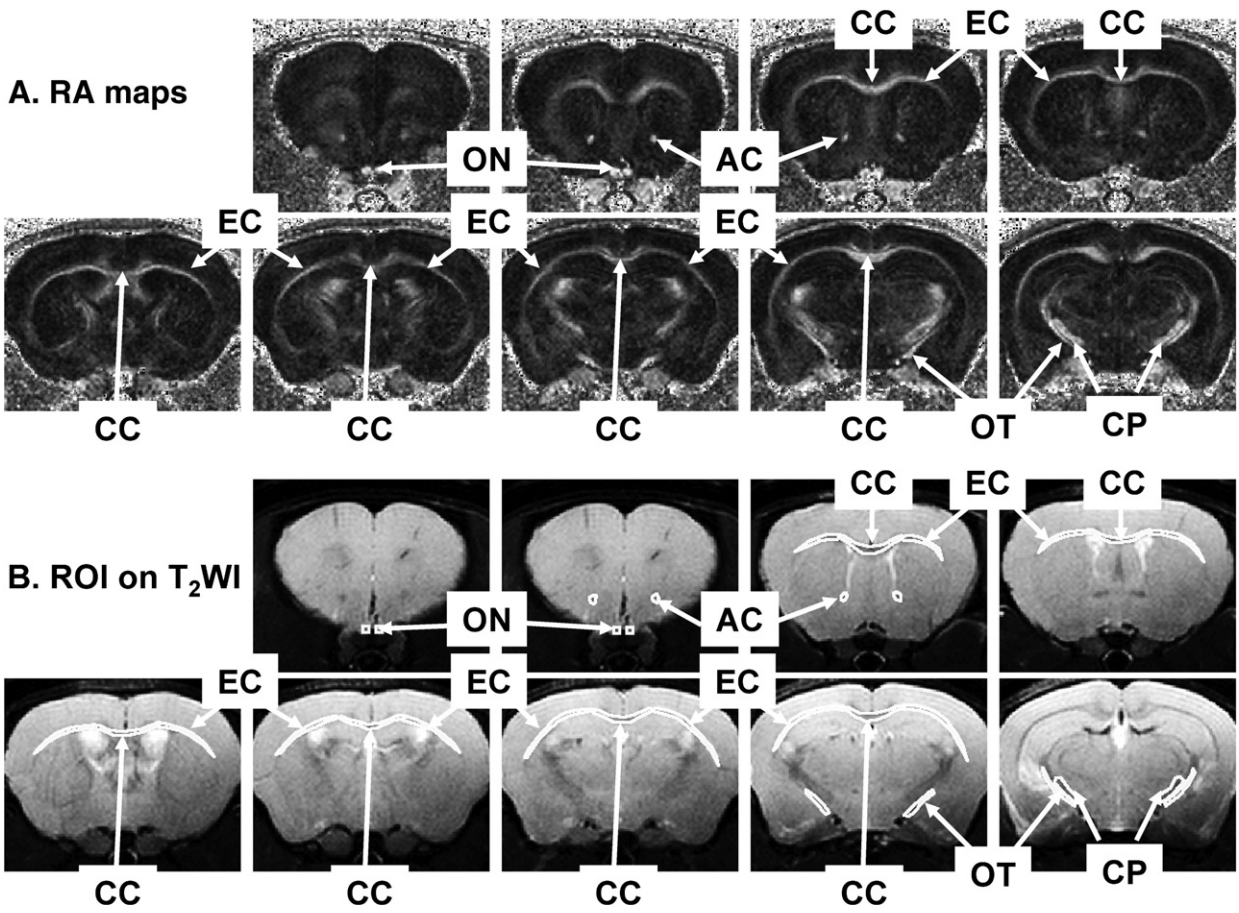

Fig. 1. White matter tracts of interest in RA (A) and T_2WI (B) maps. Six white matter tracts were examined, including anterior commissure (AC), corpus callosum (CC), cerebral peduncle (CP), external capsule (EC), optic nerve (ON), and optic tract (OT). All white matter tracts exhibit bright in RA and dark in T_2WI. The regions of interest of each white matter track were shown on the T_2WI maps.

integrity was assessed with a primary antibody against myelin basic protein (MBP, 1:250; Zymed Laboratories Inc., South San Francisco, CA) at 4 °C overnight. Following 15 min wash in PBS, sections were incubated in fluorescent secondary antibodies for 1 hr at room temperature (1:200, anti-mouse conjugated to Alexa 488 for SMI-31, 1:200, anti-rabbit conjugated to Texas Red for MBP; Molecular Probes). For every immunohistochemical examinations, two adjacent tissue sections were mounted on the same slide. One of the tissue sections went through the complete immunohistochemical staining procedures while the other was stained under the same conditions omitting the primary antibody to serve as a negative control (Aboul-Enein et al., 2006). The negative controls were performed on every immunohistochemical staining for both control and EAE tissues.

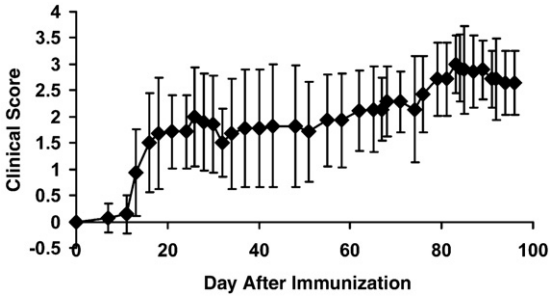

Fig. 2. Daily clinical scoring of EAE-affected mice was performed throughout the entire time course. Mice developed clinical signs approximately 13 days after immunization. The averaged clinical scores of all EAE-affected mice reached a plateau of 2.8±0.1 at approximately 83–99 days post immunization. Error bars represent standard deviations of 16 mice.

Histological sections were examined with a Nikon Eclipse 80i microscope equipped with a 60× oil objective, and digital images were captured with a Photometrics CCD digital camera using MetaMorph image acquisition software (Universal Imaging Corporation, Downington, PA). The SMI-31 and MBP positive axons were counted for each white matter tract in a blinded fashion. Specifically, images captured from the center of each white matter tract were displayed using MetaMorph. Both the green SMI-31 positive staining dot representing the normal axon and the red MBP positive staining ring representing the myelinated-axon, were counted. The axon counting was conducted through the entire captured image ($150 \times 110\ \mu m^2$). In AC, CP, EC, ON, and OT, the counts from left and right tracts were averaged to represent the counts of each tract from each mouse. The counts were presented as mean±standard deviation ($N=7$). A two-tailed *t*-test was performed to compare the measurements between control and experimental groups. The correlation coefficients of the SMI-

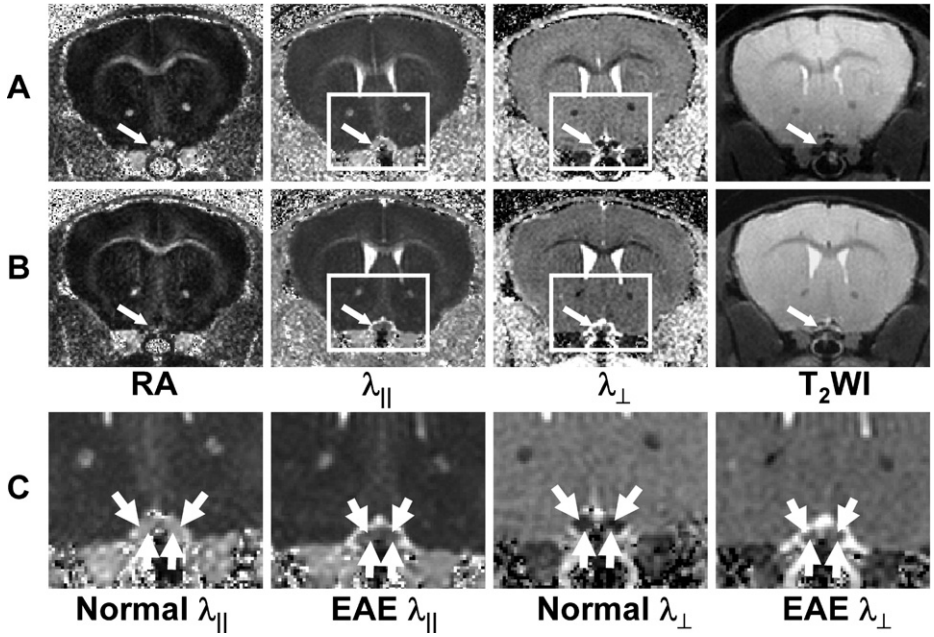

Fig. 3. Typical DTI index maps of control (A) and EAE-affected (B) optic nerves (indicated by the arrow). Expanded views of the rectangles in panels A and B are shown in panel C demonstrating decreased $\lambda_{||}$ and increased $\lambda_{\perp}$ in EAE-affected optic nerves.

31 positive counts vs. $\lambda_{||}$ and the MBP positive counts vs. $\lambda_{\perp}$ were calculated using Matlab (MathWorks, Natick, MA, USA). Statistical significance was accepted at $P<0.05$.

Results

Daily clinical scoring revealed the development of clinical signs of neurological disability approximately 13 days after immunization in the EAE group (Fig. 2, $N=16$). Three of them immediately developed severe clinical signs with scores up to 3–4 within a month and remained at that state. The rest of the group slowly and gradually deteriorated in the 3-month experimental period. The averaged clinical scores of all EAE-affected mice reached a plateau of 2.8 ± 0.1 at approximately 83–99 days post immunization.

Both the control and EAE-affected mouse brain white matter tracts exhibited higher diffusion anisotropy comparing to that of the gray matter as seen in RA maps (Figs. 3A and 4A). The decreased $\lambda_{||}$ and increased $\lambda_{\perp}$ resulted in the reduced RA in EAE-

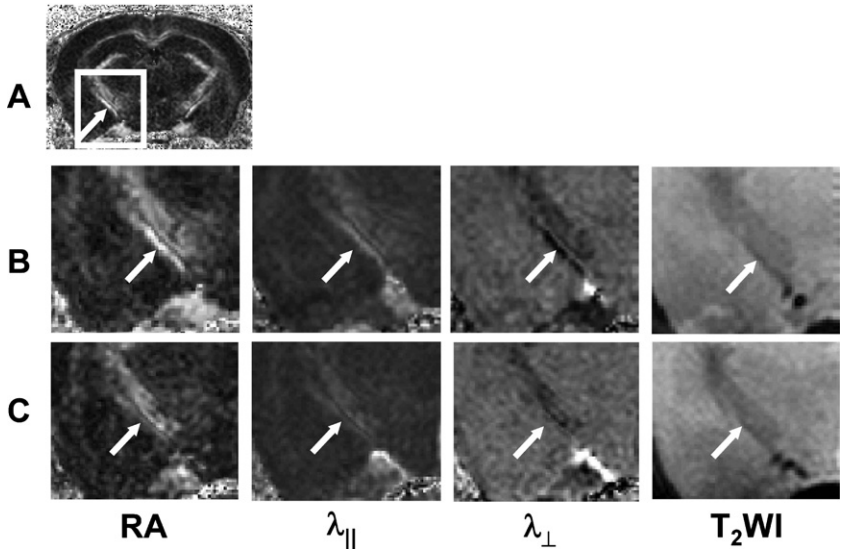

Fig. 4. Typical DTI index maps of control and EAE-affected optic tracts. A control mouse RA map is shown in panel A, where the arrow indicates the optic tract. Magnified views of the rectangles in (A) comparing the control (B), and the EAE-affected (C) mouse OT indicate decreased RA and $\lambda_{||}$, and increased $\lambda_{\perp}$ in the EAE-affected optic tracts (arrow).

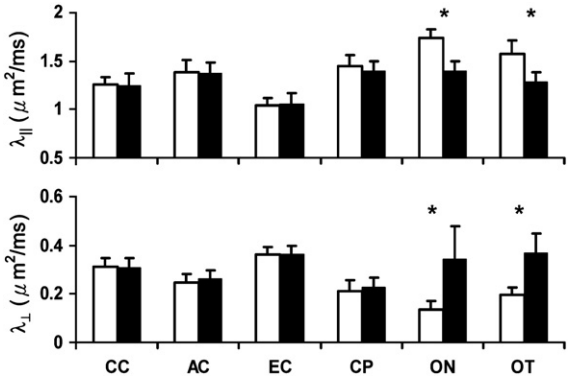

Fig. 5. Quantitative analysis of $\lambda_{||}$ and $\lambda_{\perp}$ were performed in six white matter tracts. White bars represent the measurements from the control group (control mice, $N=16$), and black bars represent the measurements from the experimental group (EAE-affected mice, $N=16$). $\lambda_{||}$ and $\lambda_{\perp}$ are given as $\mu m^2/ms \pm$ standard deviation. * Indicates statistically significant differences observed between the control and EAE mice ($P<0.05$).

affected ON (Fig. 3B) and OT (Fig. 4C) compared with that of the control (Figs. 3A and 4B). In contrast, CC and EC did not show significant changes in EAE-affected mice compared to controls (Figs. 3A and B).

Quantitative analysis showed no significant differences in $\lambda_{||}$ or $\lambda_{\perp}$ of AC, CC, CP, or EC in EAE-affected mice compared to controls 3 months after immunization (Fig. 5). However, EAE-affected ON and OT were altered with a 19% and 18% decrease in $\lambda_{||}$ ($P<0.05$) respectively (Fig. 5), suggesting the presence of axonal injury. A 156% and 86% increase in $\lambda_{\perp}$ ($P<0.05$) was also observed in ON and OT, respectively (Fig. 5), suggestive of myelin injury.

Immunohistochemistry of pNF and MBP was performed to evaluate myelin and axonal damage, respectively. The pNF and MBP staining of white matter tracts from representative EAE-affected and control mice is presented (Fig. 6). In regions of CC, AC, EC, and CP, no noticeable difference of immunohistochemistry was observed between control and EAE-affected mice. In contrast, decreased pNF and MBP were apparent in the ON and OT from EAE-affected mice suggestive of axonal and myelin damage

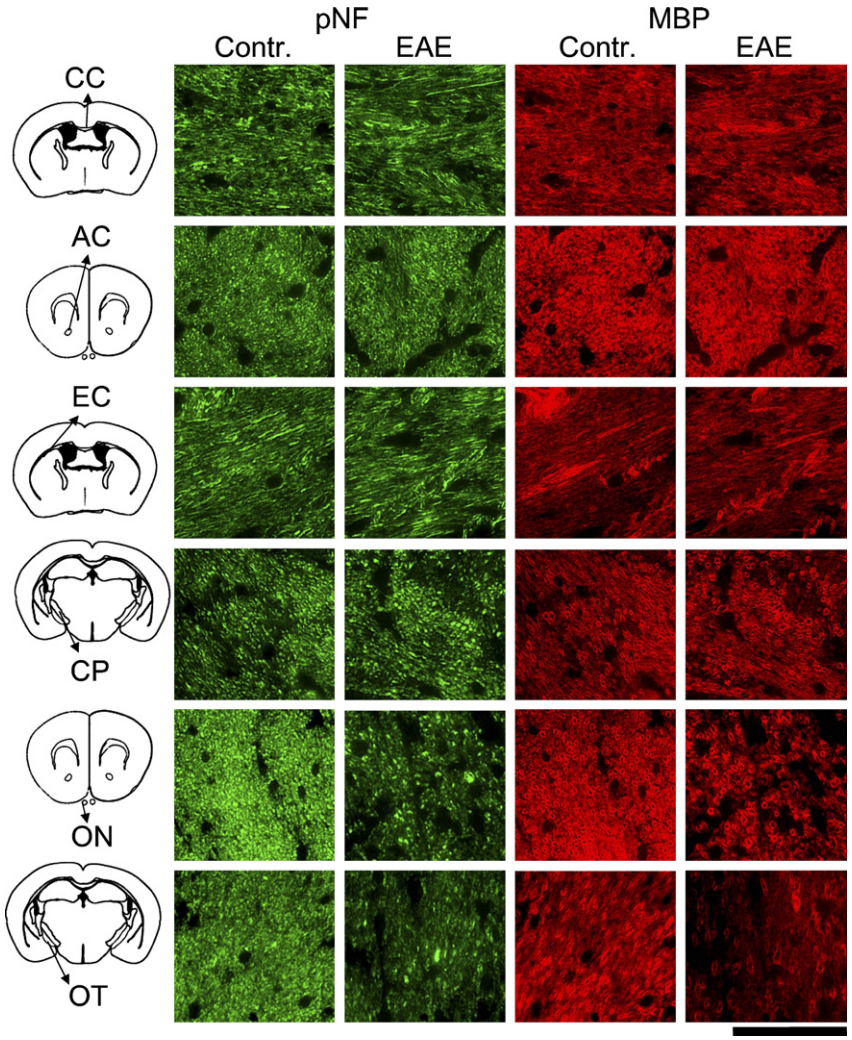

Fig. 6. Immunohistochemistry of pNF and MBP from EAE-affected and control mice. Axonal and myelin injury is seen as reduced pNF and MBP staining of the ON and OT from the EAE-affected mice. In contrast, no axonal or myelin damage was found in CC, AC, EC, and CP from the EAE-affected mice. The scale bar in the bottom right of the figure represents 30 μm.

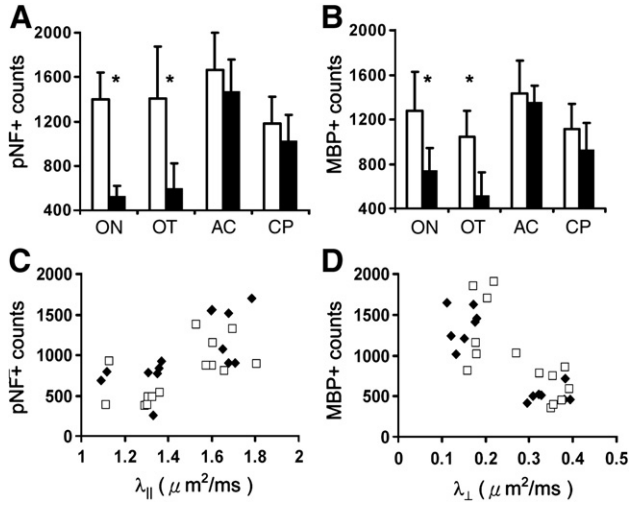

Fig. 7. The counts of pNF- (A) and MBP-positive (B) axons in optic nerve (ON), optic tract (OT), anterior commissure (AC), and cerebral peduncle (CP) from control (white bars) and EAE-affected (black bars) mice ($N=7$). The "∗" indicates $P<0.05$ for comparing measurements between control and EAE-affected mice. Significant reductions of pNF and MBP counts found in both ON and OT suggest axonal and myelin damage in both regions. In contrast, no significant changes were observed in AC or CP. The scatter plots between pNF counts vs. $\lambda_{||}$ ($r=0.642$, $P=0.002$) (C) and MBP counts vs. $\lambda_{\perp}$ ($r=-0.762$, $P=0.0004$) (D) from ON (filled symbols) and OT (opened symbols) suggest significant correlations between immunohistochemistry and DTI.

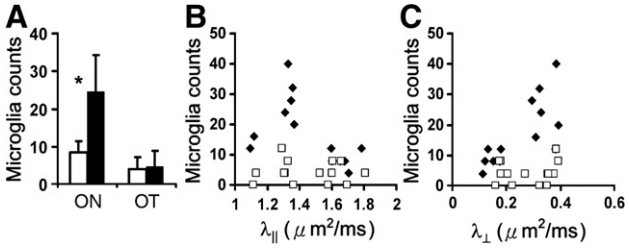

Fig. 9. The counts of microglia (A) in optic nerve (ON), optic tract (OT) from control (white bars) and EAE-affected (black bars) mice ($N=7$) and the scatter plots (B and C) between microglia counts vs. $\lambda_{||}$ and $\lambda_{\perp}$ respectively. The "*" indicates $P<0.05$ for comparing measurements between control and EAE-affected mice. Significantly increased number of microglia indicated inflammation in ON but not in OT. In the scatter plots (B and C), filled and opened symbols indicated measurements from ON and OT respectively. There is no significant correlation ($P>0.05$) between DTI indices and microglial counts.

(Fig. 6). Quantitation of immunohistochemically demonstrable pNF- and MBP-positive axons in AC, CP, ON, and OT was performed. The axon counting was not performed on CC or EC because the sections were not oriented in cross section. As shown in Fig. 7, no significant changes were observed in AC or CP. In contrast, pNF-positive axon number decreased 50 and 42% in ON and OT respectively ($N=7$, $P<0.05$); MBP positive axon numbers also decreased 62 and 58% in ON and OT respectively ($N=7$, $P<0.05$), consistent with the decreased $\lambda_{||}$ and increased $\lambda_{\perp}$. Significant correlation of pNF-positive axon numbers vs. $\lambda_{||}$ and the correlation between MBP-positive axon numbers vs. $\lambda_{\perp}$ are also demonstrated in Fig. 7. Specifically, the correlation coefficient (r) between pNF positive axon number and $\lambda_{||}$ is 0.642 with $P=0.002$, and the correlation coefficient between MBP positive axons and $\lambda_{\perp}$ is -0.762 with $P=0.0004$. The H&E staining of ON and OT also demonstrated noticeable atrophy of the ON and OT suggesting axonal damage (Fig. 8). Increased microglial infiltration

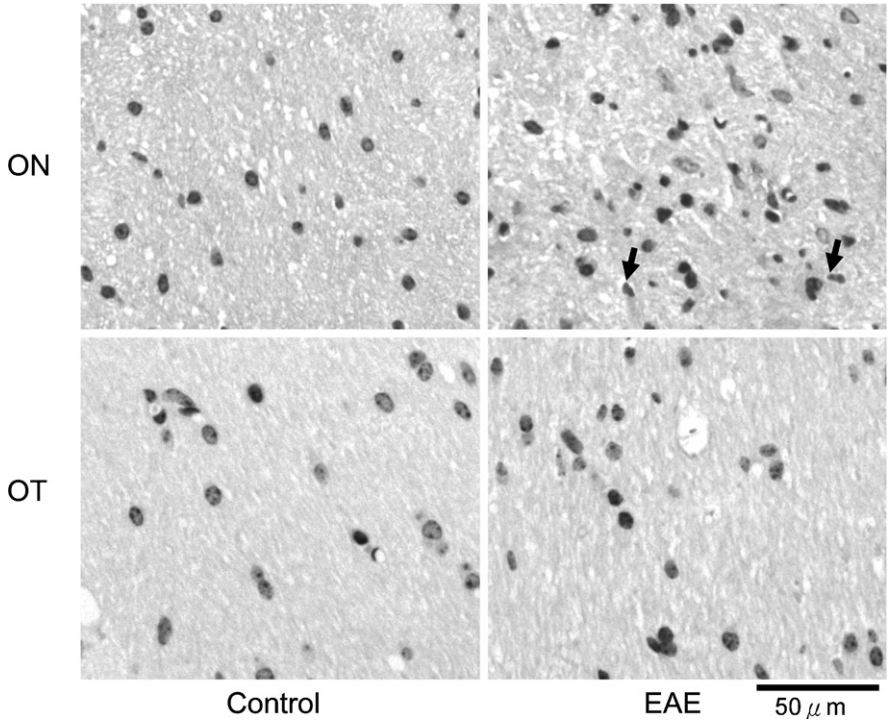

Fig. 8. H&E staining of ON and OT from control and EAE-affected mice. The infiltration of microglia, indicated by arrows, suggested the inflammatory lesion in ON co-existing with the axonal and myelin damages. However, no obvious infiltration was seen in OT.

(indicated by arrows in Fig. 8) suggests inflammation, co-existent with axonal, and myelin damages, in the ON. By counting the microglia in ON and OT respectively (Fig. 9A), a significant increase of microglia was demonstrated in ON but not in OT. The scatter plots showing the relations between directional diffusivities and microglia counts are presented in Figs. 9B and C. The increased numbers of microglia did not show a significant correlation with either $\lambda_{||}$ or $\lambda_{\perp}$. However, if ON and OT were considered separately, only ON $\lambda_{\perp}$ showed significant correlation with the microglia counts ($r=0.63$ with $P=0.016$).

Discussion

Although MS is recognized as an inflammatory demyelinating disease of the CNS with primary destruction of myelin sheaths, in reality, both demyelination and axonal injury are present in CNS white matter of MS patients. In principle, the functional deficit induced by inflammation and demyelination may be reversible. In contrast, damage to axons and neurons is likely to be irreversible once the threshold of compensation is exceeded. Thus, it has been widely speculated that axonal loss is the pathologic correlate of irreversible neurological impairment in MS (Bitsch et al., 2000; DeLuca et al., 2004; Ferguson et al., 1997; Guttmann et al., 1995; Trapp et al., 1998). On the other hand, axonal loss is not always evident in lesions from patients who are severely affected (Prineas et al., 2001). The complexity and heterogeneity of the underlying mechanisms of MS pathology require new para-clinical markers for more accurate diagnosis.

Characterizing the demyelination and axonal injury in CNS white matter is crucial for understanding MS and optimizing its treatment in patients. Currently, axon and myelin injury can be reliably distinguished only by using histological analyses (Kornek and Lassmann, 2003; Ludwin, 2000; Meier et al., 2004). However, imperfect lesion localization coupled with sampling errors and the invasive nature of such techniques limit clinical applications of histological analyses. A noninvasive method that can be used for longitudinal analysis and is capable of quantifying and differentiating axon and myelin integrity is needed and would improve the understanding and care of patients with white matter diseases. Using magnetic resonance DTI, water molecular movement along and across white matter tracts can be quantitatively expressed as axial ($\lambda_{||}$) and radial diffusivities ($\lambda_{\perp}$) respectively. Our previous studies demonstrated that decreased $\lambda_{||}$ and increased $\lambda_{\perp}$ are indicative of axon and myelin injury, respectively, in injury specific models of mouse CNS white matter damage (Song et al., 2002, 2003, 2005; Sun et al., 2005). In this study, the feasibility of using $\lambda_{||}$ and $\lambda_{\perp}$ to detect axonal and myelin damage in brain white matter of EAE-affected mice was demonstrated. The decrease in $\lambda_{||}$ and the increase in $\lambda_{\perp}$ observed in the ON and OT of EAE-affected mice suggested significant demyelination and axonal injury. The corresponding histology performed on the same tissue specimens validated the DTI findings, paving the way for using similar methods in patients with MS.

In the chronic stage of EAE presented in this study, the microglia noted in optic nerve suggests the co-existence of inflammation with axonal and myelin damage (Gonzalez-Scarano and Baltuch, 1999). Further investigations will be needed to decipher how the presence of inflammation in EAE may cause changes in the diffusion characteristics of water molecules. Although increase of $\lambda_{\perp}$ in EAE ON showed significant correlation with the microglia counts, the increase of $\lambda_{\perp}$ in EAE OT did not show a correlation with microglia counts ($r=0.18$ with $P=0.5$). The contradictory findings indicated that $\lambda_{\perp}$ may not be a marker attributing the elevated infiltration of microglia, although $\lambda_{\perp}$ may still possibly be affected by the significantly elevated infiltration of microglia. In contrast, decreased $\lambda_{||}$ correlated with the reduced SMI-31 positive axon counts and increased $\lambda_{\perp}$ correlated to the reduced MBP positive axons in both ON and OT (Fig. 7). Thus, the correlation between axonal and myelin damage with changes of $\lambda_{||}$ and $\lambda_{\perp}$ is more apparent than that of the microglia counts.

Optic neuritis is often the first clinical presentation of MS, although it can also occur as a distinct entity without subsequent or concurrent involvement of other areas of CNS myelin. A significant proportion of patients with optic neuritis eventually develop relapsing–remitting MS (Ghezzi et al., 1999; Soderstrom, 2001). Many of these patients later evolve into the secondary progressive form of MS, a more permanently debilitating stage of the disease. Animal studies could provide some insight into the selective vulnerability of the visual pathway in MS (Ghezzi et al., 1999; Guy et al., 1998; Soderstrom, 2001). The high susceptibility of the optic nerve to autoimmune damage was suggested by the distribution of the proinflammatory cytokine, tumor necrosis factor α (TNFα), in EAE-affected Lewis rats (Villarroya et al., 1996). Induction of optic neuritis in MOG-specific T cell receptor transgenic mice was also recently demonstrated (Bettelli et al., 2003). In the present study, using chronic murine EAE, *in vivo* DTI demonstrated optic tract as well as optic nerve damage. The myelin and axonal damage to the optic tract may be secondary to the extensive degeneration of the optic nerve. Alternatively, it is also possible that the optic tract itself is independently susceptible to EAE induced injury.

In this study, diffusion weighting factor (b) of 0.847 ms/μm^2 was used for DTI data acquisition. This is consistent with the current practice in human brain DTI measurements where b is commonly set ranging from 0.6 to 1 ms/μm^2 (Mori et al., 2002; Pierpaoli et al., 1996). The choice of a b value smaller than 1 ms/μm^2 was to minimize the estimation errors for fitting the data to the mono-exponential diffusion tensor model in this study (Basser and Pierpaoli, 1996; Clark et al., 2002; Jones, 2004). The use of minimal diffusion weighting, 6-independent non-colinear directions (Basser and Pierpaoli, 1998; Ozcan, 2005), herein was to minimize the acquisition time with sufficient image resolution and quality (Song et al., 2002, 2003, 2005; Sun et al., 2003, 2005, 2006a,b).

Given the diffusion measurement sampling the motion of water molecules in the order of 10 μm, the mouse respiratory motion causing bulk movement in the order of mm would result in insurmountable obstacles in tensor calculation. In this study, the head holder developed in our lab was employed to immobilize the mouse head eliminating the motion artifacts resulting from respiration (Song et al., 2002, 2003, 2005; Sun et al., 2003, 2005, 2006a,b). In recent reports, pulsations of cerebral tissues resulting from cardiac contraction have been reported to cause errors in human brain DTI measurements (Conturo et al., 1995; Enzmann and Pelc, 1992; Poncelet et al., 1992; Turner et al., 1990). However, the pulsation effects seen in human brain has not been observed in mouse brain or spinal cord as evident in that comparable diffusion anisotropy was observed in mouse brain and spinal cord *in vivo* and *ex vivo* after death and fixation (Kim et al., 2007; Sun et al., 2003).

The slice thickness of 0.5 mm employed in this study represents the highest *in vivo* DTI measurements from the mouse brains with

the reported slice thickness ranging from 0.5 to 1 mm in the literature (Ahmad et al., 2005; Boretius et al., 2007; Guilfoyle et al., 2003; Harsan et al., 2006, 2007; Nair et al., 2005; Sow et al., 2006). However, mouse optic tract measures roughly 0.6 mm thick (Franklin and Paxinos, 1997) suggesting that 0.5-mm-thick DTI maps will suffer the unavoidable partial volume effect. Nevertheless, the consistency between the DTI estimated injury and the histology findings suggests that the partial volume effect may not adversely affect our results. This may be partially due to the carefully and reproducibly planed image slices using the exact anatomical landmarks on the sagittal and axial scouts of each mouse brain ensuring a consistent slice location of the tract from all mice examined. Thus, the partial volume effect in the current study may be quite comparable for both control and EAE mice. It is also possible that the gray matter in EAE mice may not be significantly affected in this model thus contributing insignificantly to the observed DTI changes. It is apparent that the partial volume effect did not diminish the capability of DTI to detect the damage caused by EAE presented in this study although one has to keep the partial volume effect into account in more detailed mechanistic studies.

Derived from diffusion tensor matrix, the largest eigenvalue and the associated eigenvector (λ_1 and v_1) have been shown to represent the diffusion magnitude and direction parallel to the white matter tract and have been used in tractography in the CNS of both human and animal models (Jones and Pierpaoli, 2005; Le Bihan et al., 2001; Mori and van Zijl, 2002). Thus, $\lambda_{\|}$ and $\lambda_{\perp}$ for quantifying respectively diffusivities parallel and perpendicular to the white matter tract is consistent with the current application of DTI in the field. However, possibilities do exist that the loss of integrity in the white matter tracts, such as severe axon and myelin loss, or fiber crossing resulting in relatively isotropic water diffusion. Consequently, λ_1, λ_2, and λ_3 would become nearly indistinguishable and the theoretical basis of the directional diffusion and white matter structure will no longer hold. The tissue disintegration seen as progressive equalization of $\lambda_{\|}$ and $\lambda_{\perp}$ in longitudinal measurements may suggest that the proposed use of differentiating axonal and myelin injury under such conditions would be inappropriate.

However, such extreme case is not likely to reflect the EAE pathology observed in the present study. Specifically, $\lambda_{\|}$ reduced from a control value of 1.6 μm^2/ms to 1.3 μm^2/ms while $\lambda_{\perp}$ increased from the control value of 0.15 μm^2/ms to 0.35 μm^2/ms in the chronic EAE. In the chronic stage, where the axonal and myelin damage is expected to be more severe than the one in acute state, the visual pathway $\lambda_{\|}$ is still 3.7 times of $\lambda_{\perp}$. This ratio between $\lambda_{\|}$ and $\lambda_{\perp}$ is in agreement with previously reported results from *in vivo* mouse brains (Song et al., 2002, 2003, 2005; Sun et al., 2003, 2005, 2006a,b).

Our group has employed various pathology specific mouse models of white matter injury to test the utility of $\lambda_{\|}$ and $\lambda_{\perp}$ for detecting and differentiating axonal and myelin damages previously. Specifically, in the mouse models of axonal damage only (the Wallerian degeneration of optic nerve at 3 days after retinal ischemia) (Song et al., 2003; Sun et al., 2006a), myelin damage only (cuprizone induced myelin damage in corpus callosum and the dysmyelinated white matter of shiverer mice) (Song et al., 2002, 2005; Sun et al., 2006b), and the coexistence of axonal and myelin damage (the Wallerian degeneration in optic nerve at 14 days after retinal ischemia) (Song et al., 2003; Sun et al., 2006a), decreased $\lambda_{\|}$ and increased $\lambda_{\perp}$ proved to be capable of accurately detecting and differentiating axonal and myelin damages respectively. In this study, the application of $\lambda_{\|}$ and $\lambda_{\perp}$ to detect the underlying axonal and myelin injury in white matter from EAE-affected mice was attempted as the first test of the utility of this proposed method in a more clinically relevant condition where a mixed pathological situation is encountered. As a result, $\lambda_{\|}$ and $\lambda_{\perp}$ clearly detected the axonal and myelin injury of the optic nerve and tract from EAE-affected mice. The injured and uninjured white matter tracts identified using $\lambda_{\|}$ and $\lambda_{\perp}$ positively correlated with findings of immunohistochemisty despite the complicated EAE pathology.

In conclusion, this study demonstrated the feasibility of using decreased $\lambda_{\|}$ and increased $\lambda_{\perp}$ as biomarkers of axonal and myelin injury respectively in a murine model of MS. Selective injury of the optic nerve and tract in EAE-affected mice was demonstrated non-invasively and is consistent with corresponding histology and the literature findings. Use of directional diffusivities as applied in the present study is readily applicable to human MS since DTI technology has become widely available in most hospitals. These methods could play a significant role in stratification and efficacy assessment of intervention, and monitoring the progression of the disease.

Acknowledgments

We thank the valuable and important statistical analysis and suggestions from Dr. Kathryn Trinkaus, Division of Biostatistics, Washington University School of Medicine. We also thank the supports from NMSS RG-3864 and CA-1012, and NIH R01-NS-047592 and R01-NS-054194.

References

Aboul-Enein, F., et al., 2006. Transient axonal injury in the absence of demyelination: a correlate of clinical disease in acute experimental autoimmune encephalomyelitis. Acta Neuropathol. (Berl.) 111, 539–547.

Ahmad, I., et al., 2005. Allopregnanolone treatment, both as a single injection or repetitively, delays demyelination and enhances survival of Niemann–Pick C mice. J. Neurosci. Res. 82, 811–821.

Basser, P.J., Pierpaoli, C., 1996. Microstructural and physiological features of tissues elucidated by quantitative-diffusion-tensor MRI. J. Magn. Reson., B 111, 209–219.

Basser, P.J., Pierpaoli, C., 1998. A simplified method to measure the diffusion tensor from seven MR images. Magn. Reson. Med. 39, 928–934.

Bettelli, E., et al., 2003. Myelin oligodendrocyte glycoprotein-specific T cell receptor transgenic mice develop spontaneous autoimmune optic neuritis. J. Exp. Med. 197, 1073–1081.

Bitsch, A., et al., 2000. Acute axonal injury in multiple sclerosis. Correlation with demyelination and inflammation. Brain 123 (Pt 6), 1174–1183.

Boretius, S., et al., 2007. High-field diffusion tensor imaging of mouse brain in vivo using single-shot STEAM MRI. J. Neurosci. Methods 161, 112–117.

Clark, C.A., et al., 2002. In vivo mapping of the fast and slow diffusion tensors in human brain. Magn. Reson. Med. 47, 623–628.

Conlon, P., et al., 1999. The immunobiology of multiple sclerosis: an autoimmune disease of the central nervous system. Neurobiol. Dis. 6, 149–166.

Conturo, T.E., et al., 1995. Diffusion MRI: precision, accuracy and flow effects. NMR Biomed. 8, 307–332.

Craner, M.J., et al., 2005. Sodium channels contribute to microglia/macrophage activation and function in EAE and MS. Glia 49, 220–229.

Cross, A.H., et al., 1994. Aminoguanidine, an inhibitor of inducible nitric oxide synthase, ameliorates experimental autoimmune encephalomyelitis in SJL mice. J. Clin. Invest. 93, 2684–2690.
Davie, C.A., et al., 1997. 1H magnetic resonance spectroscopy of chronic cerebral white matter lesions and normal appearing white matter in multiple sclerosis. J. Neurol. Neurosurg. Psychiatry 63, 736–742.
DeLuca, G.C., et al., 2004. Axonal loss in multiple sclerosis: a pathological survey of the corticospinal and sensory tracts. Brain 127, 1009–1018.
Enzmann, D.R., Pelc, N.J., 1992. Brain motion: measurement with phase-contrast MR imaging. Radiology 185, 653–660.
Ferguson, B., et al., 1997. Axonal damage in acute multiple sclerosis lesions. Brain 120 (Pt 3), 393–399.
Franklin, K.B., Paxinos, G., 1997. The Mouse Brain in Stereotaxic Coordinates. Academic Press, San Diego.
Fu, L., et al., 1998. Imaging axonal damage of normal-appearing white matter in multiple sclerosis. Brain 121 (Pt 1), 103–113.
Ghezzi, A., et al., 1999. Long-term follow-up of isolated optic neuritis: the risk of developing multiple sclerosis, its outcome, and the prognostic role of paraclinical tests. J. Neurol. 246, 770–775.
Gonzalez-Scarano, F., Baltuch, G., 1999. Microglia as mediators of inflammatory and degenerative diseases. Annu. Rev. Neurosci. 22, 219–240.
Guilfoyle, D.N., et al., 2003. Diffusion tensor imaging in fixed brain tissue at 7.0 T. NMR Biomed. 16, 77–81.
Guttmann, C.R., et al., 1995. The evolution of multiple sclerosis lesions on serial MR. AJNR Am. J. Neuroradiol. 16, 1481–1491.
Guy, J., et al., 1998. Adeno-associated viral-mediated catalase expression suppresses optic neuritis in experimental allergic encephalomyelitis. Proc. Natl. Acad. Sci. U. S. A. 95, 13847–13852.
Harsan, L.A., et al., 2006. Brain dysmyelination and recovery assessment by noninvasive in vivo diffusion tensor magnetic resonance imaging. J. Neurosci. Res. 83, 392–402.
Harsan, L.A., et al., 2007. Astrocytic hypertrophy in dysmyelination influences the diffusion anisotropy of white matter. J. Neurosci. Res. 85, 935–944.
Iglesias, A., et al., 2001. T- and B-cell responses to myelin oligodendrocyte glycoprotein in experimental autoimmune encephalomyelitis and multiple sclerosis. Glia 36, 220–234.
Jones, D.K., 2004. The effect of gradient sampling schemes on measures derived from diffusion tensor MRI: a Monte Carlo study. Magn. Reson. Med. 51, 807–815.
Jones, D.K., Pierpaoli, C., 2005. Confidence mapping in diffusion tensor magnetic resonance imaging tractography using a bootstrap approach. Magn. Reson. Med. 53, 1143–1149.
Kim, J.H., et al., 2006. Detecting axon damage in spinal cord from a mouse model of multiple sclerosis. Neurobiol. Dis. 21, 626–632.
Kim, J.H., et al., 2007. Postmortem delay does not change regional diffusion anisotropy characteristics in mouse spinal cord white matter. NMR Biomed. 20, 352–359.
Kornek, B., Lassmann, H., 2003. Neuropathology of multiple sclerosis—New concepts. Brain Res. Bull. 61, 321–326.
Kornek, B., et al., 2000. Multiple sclerosis and chronic autoimmune encephalomyelitis: a comparative quantitative study of axonal injury in active, inactive, and remyelinated lesions. Am. J. Pathol. 157, 267–276.
Le Bihan, D., et al., 2001. Diffusion tensor imaging: concepts and applications. J. Magn. Reson. Imaging 13, 534–546.
Linington, C., et al., 1993. T cells specific for the myelin oligodendrocyte glycoprotein mediate an unusual autoimmune inflammatory response in the central nervous system. Eur. J. Immunol. 23, 1364–1372.
Ludwin, S.K., 2000. The neuropathology of multiple sclerosis. Neuroimaging Clin. N. Am. 10, 625–648 vii.
Lyons, J.A., et al., 1999. B cells are critical to induction of experimental allergic encephalomyelitis by protein but not by a short encephalitogenic peptide. Eur. J. Immunol. 29, 3432–3439.
Meier, D.S., et al., 2004. Magnetic resonance imaging surrogates of multiple sclerosis pathology and their relationship to central nervous system atrophy. J. Neuroimaging 14, 46S–53S.
Mori, S., van Zijl, P.C., 2002. Fiber tracking: principles and strategies—A technical review. NMR Biomed. 15, 468–480.
Mori, S., et al., 2002. Imaging cortical association tracts in the human brain using diffusion-tensor-based axonal tracking. Magn. Reson. Med. 47, 215–223.
Morrissey, S.P., et al., 1996. In vivo MRI and its histological correlates in acute adoptive transfer experimental allergic encephalomyelitis. Quantification of inflammation and oedema. Brain 119 (Pt 1), 239–248.
Nair, G., et al., 2005. Myelination and long diffusion times alter diffusion-tensor-imaging contrast in myelin-deficient shiverer mice. NeuroImage 28, 165–174.
Ozcan, A., 2005. (Mathematical) Necessary conditions for the selection of gradient vectors in DTI. J. Magn. Reson. 172, 238–241.
Pierpaoli, C., et al., 1996. Diffusion tensor MR imaging of the human brain. Radiology 201, 637–648.
Poncelet, B.P., et al., 1992. Brain parenchyma motion: measurement with cine echo-planar MR imaging. Radiology 185, 645–651.
Prineas, J.W., et al., 2001. Immunopathology of secondary-progressive multiple sclerosis. Ann. Neurol. 50, 646–657.
Raine, C.S., 1984. Biology of disease. Analysis of autoimmune demyelination: its impact upon multiple sclerosis. Lab. Invest. 50, 608–635.
Raine, C.S., Traugott, U., 1984. Experimental autoimmune demyelination. Chronic relapsing models and their therapeutic implications for multiple sclerosis. Ann. N. Y. Acad. Sci. 436, 33–51.
Rovaris, M., Filippi, M., 2000. Contrast enhancement and the acute lesion in multiple sclerosis. Neuroimaging Clin. N. Am. 10, 705–716 viii–ix.
Soderstrom, M., 2001. Optic neuritis and multiple sclerosis. Acta Ophthalmol. Scand. 79, 223–227.
Song, S.K., et al., 2002. Dysmyelination revealed through MRI as increased radial (but unchanged axial) diffusion of water. NeuroImage 17, 1429–1436.
Song, S.K., et al., 2003. Diffusion tensor imaging detects and differentiates axon and myelin degeneration in mouse optic nerve after retinal ischemia. NeuroImage 20, 1714–1722.
Song, S.K., et al., 2005. Demyelination increases radial diffusivity in corpus callosum of mouse brain. NeuroImage 26, 132–140.
Sow, A., et al., 2006. Oligodendrocyte differentiation is increased in transferrin transgenic mice. J. Neurosci. Res. 83, 403–414.
Storch, M.K., et al., 1998. Autoimmunity to myelin oligodendrocyte glycoprotein in rats mimics the spectrum of multiple sclerosis pathology. Brain Pathol. 8, 681–694.
Sun, S.W., et al., 2003. Relative indices of water diffusion anisotropy are equivalent in live and formalin-fixed mouse brains. Magn. Reson. Med. 50, 743–748.
Sun, S.W., et al., 2005. Detection of age-dependent brain injury in a mouse model of brain amyloidosis associated with Alzheimer's disease using magnetic resonance diffusion tensor imaging. Exp. Neurol. 191, 77–85.
Sun, S.W., et al., 2006a. Differential sensitivity of in vivo and ex vivo diffusion tensor imaging to evolving optic nerve injury in mice with retinal ischemia. NeuroImage 32, 1195–1204.
Sun, S.W., et al., 2006b. Noninvasive detection of cuprizone induced axonal damage and demyelination in the mouse corpus callosum. Magn. Reson. Med. 55, 302–308.
Trapp, B.D., et al., 1998. Axonal transection in the lesions of multiple sclerosis. N. Engl. J. Med. 338, 278–285.
Turner, R., et al., 1990. Echo-planar imaging of intravoxel incoherent motion. Radiology 177, 407–414.
Villarroya, H., et al., 1996. Myelin-induced experimental allergic encephalomyelitis in Lewis rats: tumor necrosis factor alpha levels in serum and cerebrospinal fluid immunohistochemical expression in glial cells and macrophages of optic nerve and spinal cord. J. Neuroimmunol. 64, 55–61.
Whitney, L.W., et al., 1999. Analysis of gene expression in multiple sclerosis lesions using cDNA microarrays. Ann. Neurol. 46, 425–428.
Yousry, I., et al., 2000. Serial gadolinium–DTPA of spinal cord MRI in multiple sclerosis: triple vs. single dose. Magn. Reson. Imaging 18, 1183–1186.